JOURNAL OF GEOPHYSICAL RESEARCH, VOL. 85, NO. C2, PAGES 1085–1094, FEBRUARY 20, 1980

Description of Nonlinear Internal Wave Interactions Using Langevin Methods

NEIL POMPHREY, JAMES D. MEISS, AND KENNETH M. WATSON

Department of Physics and Lawrence Berkeley Laboratory
University of California, Berkeley, California 94720

A comparison is made between several methods for calculating energy transport among the linear normal modes of the internal wave field. Two Langevin techniques are presented. The first is based on the fluctuation-dissipation theorem and provides a relaxation rate ν_F and a transport equation. The second method is an application of the Krylov-Bogoliubov-Mitropolsky perturbation theory and provides a Langevin rate constant ν_P calculated here only to lowest order. The two formulations are closely related to the radiative transfer (Boltzmann) equation, whose rate is the difference between ν_F and ν_P. Computations confirm the conclusion of McComas and Bretherton that the GM-76 spectrum is approximately a steady state spectrum for three-wave interactions except for frequencies near the inertial frequency and at the lowest vertical modenumbers. The sensitivity of ν_F and ν_P to spectral form is also discussed. Simple analytic expressions for the rates are derived for the induced diffusion, elastic scattering, and parametric subharmonic instability mechanisms. The first of these expressions provides a useful fit to the full computation over much of the spectrum. Finally, net energy flow in the nonequilibrium portion of the GM-76 spectrum is discussed.

1. INTRODUCTION

Nonlinear energy transfer mechanisms within the oceanic internal wave field have been studied by *Olbers* [1976] and *McComas and Bretherton* [1977]. These authors used a radiative transfer equation [*Hasselmann*, 1966, 1967] for their computations. The radiative transfer (or Boltzmann) equation governs the evolution of wave action spectra ensemble averaged over many realizations of the wave field. Derivation of this equation from the fluid equations requires several approximations: (a) nonlinearities are assumed 'weak,' and only lowest-order (quadratic for the case of internal waves) nonlinear terms are retained in the equations of motion; (b) two-time perturbation methods are used; the 'fast time' corresponds to linear wave periods and the 'slow time' to nonlinear interaction time scales; (c) spatial homogeneity in any horizontal plane is assumed. This allows simplification of second moments of wave amplitudes; and (d) a closure approximation is made by the discard of fourth and higher-order cumulants.

In the present study we compare several different techniques for calculating energy transport within the internal wave field. The dynamical equations (*Meiss et al.*, [1979] henceforth referred to as paper 1) are derived using approximation (a) and describe nonlinear interaction of the linear normal modes of the wave field. Here we use the Garrett-Munk exponential profile for the Väisälä frequency and the WKB approximation to calculate the vertical modefunctions. Our modal picture contrasts with the work of *Olbers* [1976] and *McComas and Bretherton* [1977], who used a formulation based on progressive waves. The relation between the two descriptions is outlined in Appendix A. Two Langevin equation techniques are developed in this paper to study the dynamics of the system derived in paper 1 (Langevin methods have been used by *Holloway and Hendershott* [1977] to discuss Rossby waves).

The first Langevin method is based on the fluctuation-dissipation theorem [*Lax*, 1960, 1966]. This method provides relaxation rates and a transport equation and depends rather little on dynamics. It assumes linear relaxation to a 'known equilibrium' state and also requires approximations (b), (c), and (d).

To obtain the second form of the Langevin equation, we use approximation (b) in the form of the Krylov-Bogoliubov-Mitropolsky perturbation method, which yields directly an equation of the Langevin form [*Bogoliubov and Mitropolsky*, 1961]. Approximation (d) is not required to calculate the Langevin rate constant with this procedure.

We shall show in section 3 that the two Langevin formulations are closely related to the radiative transfer equation. For fluctuations near a steady state the two formulations are in agreement. In this case the transport equation obtained from the Langevin equation is identical in form with that used by *Olbers* [1976] and by *McComas and Bretherton* [1977].

The Langevin methods lead to a decay rate $\nu(k)$ for the autocorrelation of the amplitude for a linear internal wave labeled as 'k.' When calculated using the fluctuation-dissipation theorem, we call this $\nu_F(k)$. The value obtained from perturbation theory is written as $\nu_P(k)$. The radiative transfer equation used by *Olbers* [1976] and by *McComas and Bretherton* [1977] for the action density $\langle J_k \rangle$ can be written in the form

$$\frac{d}{dt}\langle J_k \rangle = 2\nu_B(k)\langle J_k \rangle$$

The Boltzmann rate is shown to be related to the Langevin rates by

$$\nu_B(k) = \nu_F(k) - \nu_P(k)$$

It is convenient to think of ν_F as representing the rate of energy input to mode k from the 'noise field' of the wave system and to think of ν_P as describing a rate of energy loss from mode k.

McComas [1978] reported numerical experiments in which he introduced small distortions in the GM-76 spectrum and computed the relaxation to 'equilibrium.' We give an analytic description of this in section 3, observing that the Langevin rate $\nu_P(k)$ determines the rate of return to equilibrium.

Numerical calculations of ν_F and ν_P for a set of Garrett-Munk related spectra (with GM-76 as our reference standard) are presented in section 5. We shall see that for the GM-76

Paper number 9C1429.
0148-0227/80/009C-1429$01.00

spectrum, except for frequencies near the inertial frequency and at the lowest vertical mode numbers, $|\nu_B|$ is from 1–3 orders of magnitude smaller than ν_F (or ν_P). We thus find precise numerical confirmation of the conclusion of *McComas and Bretherton* [1977] (who calculate only ν_B) that GM-76 is approximately a steady state in this region. Not surprisingly, in the equilibrium region where ν_B is a small difference between two much larger quantities, the values of ν_B are rather sensitive to spectral shape.

McComas and Bretherton [1977] describe three limiting mechanisms for energy transfer. They call these induced diffusion, elastic scattering, and parametric subharmonic instability. In section 6 we show that GM-76 represents a steady state except at the lowest frequencies and lowest vertical mode numbers, with respect to both induced diffusion and elastic scattering. (For the case of induced diffusion this was noted by *McComas and Bretherton* [1977] and was implied more generally from their numerical calculations). We also present simple analytic expressions for ν_F and ν_P for each of the three mechanisms. For frequencies greater than 3 times the inertial frequency the analytic expressions obtained from induced diffusion for both ν_F and ν_P agree well with the numerically calculated values for these quantities. The elastic scattering contribution is an order of magnitude smaller. For frequencies less than about twice the inertial frequency our approximate expression for the parametric subharmonic instability rate accounts for a significant fraction of the total rate.

Net energy flow in the nonequilibrium portion of the GM-76 spectrum is discussed in section 7. Our conclusions are generally consistent with those of *Olbers* [1976] and of *McComas and Bretherton* [1977] that energy is transferred from the low vertical mode number regime into that of high vertical mode numbers and near inertial frequencies. Since net energy flow is determined by ν_B, the details depend relatively sensitively on the assumed spectrum.

The Langevin rate constants discussed here govern relaxation processes in the wave field and also immediately yield values for the more frequently calculated Boltzmann constant ν_B. The simple analytic approximations for these rate constants given in this paper should be adequate for applications to internal wave transport processes.

2. The Dynamical Model

A general description of internal wave phenomena and theory is given by *Phillips* [1977]. The detailed description of the specific dynamical model used here is given in paper 1. A rectangular coordinate system is chosen with the x-y plane tangent (locally) to the ocean surface. The bottom is assumed horizontal at $z = -H$. The Garrett-Munk exponential Väisälä profile is used in this paper:

$$N(z) = N_0 \exp(z/B) \tag{1}$$

Dimensional quantities are $N_0 = 5.2\ (10)^{-3}$ rad/s, $B = 1.2$ km, and the surface fluid density $\rho_0 = \rho(0)$. The coriolis frequency is assumed vertical with magnitude

$$f = 7.3\ (10)^{-5}\ \text{rad/s} = 0.014\ N_0 \tag{2}$$

corresponding to 30° latitude. Vectors, $\mathbf{x} = (x, y)$, are two-dimensional in the horizontal plane.

The vertical displacement of a Lagrangian fluid element was written in paper 1 as

$$\xi_3(\mathbf{x}, z, t) = \text{Re}\ [Y(\mathbf{x}, z, t)]$$

$$Y(\mathbf{x}, z, t) = iN_0(B)^{1/2} \sum_{\alpha=1}^{\infty} \sum_{\mathbf{k}} \frac{a_{\mathbf{k}\alpha}(t)}{k} W_{k\alpha}(z) e^{i\mathbf{k}\cdot\mathbf{x}} \tag{3}$$

Equation (3) is a Fourier expansion in an ocean of rectangular area $\sum_0$ in terms of horizontal wave numbers $\mathbf{k}$. The linear vertical mode functions, $W_{k\alpha}(z)$, satisfy the eigenvalue equation

$$\frac{d}{dz}\left[\rho \frac{d}{dz} W_{k\alpha}\right] + \rho k^2 \left[\frac{N^2 - \omega_\alpha^2(k)}{\omega_\alpha^2(k) - f^2}\right] W_{k\alpha} = 0 \qquad \omega_\alpha(k) > 0$$

$$W_{k\alpha}(0) = W_{k\alpha}(-H) = 0 \tag{4}$$

Here $\omega_\alpha(k)$ is the angular frequency of a linear internal wave with integer vertical modenumber α.

The amplitudes $a_{\mathbf{k}\alpha}$ are dimensionless wave slope variables and satisfy (paper 1, equation (2.23))

$$\dot{a}_k + i\omega_\alpha a_k = \sum_{l,m} [\delta_{\mathbf{k}+\mathbf{l}-\mathbf{m}} G_m{}^{kl} a_l^* a_m + \delta_{\mathbf{k}-\mathbf{l}-\mathbf{m}} G_{lm}{}^{k} a_l a_m] \tag{5}$$

Here we have used abbreviated labels, writing k, l, m for $(\mathbf{k}, \alpha)$, $(\mathbf{l}, \beta)$, and $(\mathbf{m}, \gamma)$, respectively. Explicit expressions for the 'G' coupling coefficients in (5) were given in paper 1. They contain integrals over the product of three mode functions W (see Appendix A) as well as factors determined by the geometry of the interacting triad.

Wave action per unit area is expressed in terms of the slope variables as (paper 1, equation (2.21))

$$J_{\mathbf{k}\alpha} = \rho_0 N_0 B^3 \frac{\omega_\alpha N_0}{\omega_\alpha^2 - f^2} \frac{|a_{\mathbf{k}\alpha}|^2}{2(kB)^2} \tag{6}$$

The Boussinesq approximation has not been used to derive (3), (4), and (5). This approximation entails the neglect of the term $d\rho/dz\ dW_{k\alpha}/dz$ in (4). In Appendix A it is shown to have a negligible effect on the coupling coefficients in (5). We shall therefore make this simplifying approximation for our subsequent discussion.

Following *Garrett and Munk* [1975, 1979], we use the WKB approximation to solve (4). This appears reasonably valid for $\alpha \geq 2$ (results for $\alpha = 1$ are at best qualitative but will be included for completeness). We also use their dispersion relation

$$\omega_\alpha^2(k) = f^2 + \left(\frac{kBN_0}{(\alpha - \frac{1}{2})\pi}\right)^2 \tag{7}$$

valid when $\omega_\alpha(k) \ll N_0$ (and assumed valid in this paper for $\omega_\alpha(k) < N_0/3$).

The power spectral density (PSD) of vertical displacement is written as $\psi(\mathbf{k}, \alpha, z)$ and normalized so that

$$\langle \xi_3^2 \rangle = \sum_{\alpha=1}^{\infty} \int d^2k\ \psi(\mathbf{k}, \alpha, z) \tag{8}$$

where angle brackets represents an ensemble average over realizations of the internal wave field. We shall require only the spectrum $\psi(\mathbf{k}, \alpha)$ extrapolated to the surface for which $\langle \xi_3^2 \rangle = \langle \xi_0^2 \rangle = (7.3\ \text{m})^2$. From (1), (3), (6), (7), and the normalization of the eigenfunctions $W_{k\alpha}$ (Appendix A), we see that

$$\psi(\mathbf{k}, \alpha) = \frac{\sum_0 \langle |a_{\mathbf{k}\alpha}|^2 \rangle}{4\pi^2} \frac{}{2k^2} \tag{9}$$

In this paper we adopt a PSD related to the Garrett-Munk form [*Garrett and Munk*, 1975, 1979], with

$$\psi(\mathbf{k}, \alpha) = \frac{1}{2\pi} N_{pt} \langle (\xi_0 B)^2 \rangle \left\{ \frac{(kB)\alpha^{p-1}}{[(kB)^2 + 1.9(10)^{-3}\alpha^2]^{p/2+1}[1 + (\alpha/3)^t]} \right\} \tag{10}$$

where p is the 'wave number slope' and t is the 'mode number slope.' The GM-76 spectrum [*Cairns and Williams*, 1976] with $p = 2$, $t = 2$, and $N_{22} = 0.013$ is chosen as our 'standard.'

3. Relaxation Rates

In this section we discuss and relate three different methods for calculating relaxation rates in a random wave field. We fix attention on a single, definite internal wave mode, say that labeled $(\mathbf{k}, \alpha)$. This is the 'test wave,' and we study its interaction with the ambient wavefield. Averages are denoted by angle brackets and are over an ensemble of states of the ambient field. We suppose that the test wave always has a definite amplitude at some initial time, say $t = 0$. As $t \to \infty$, there will be no difference between this ensemble and an ensemble of states of the entire internal wave field (including the test wave).

Fluctuation Dissipation Theorem

We cast the equations of motion (5) for the test wave as a Langevin equation by representing the nonlinear terms on the right-hand side by random force $\tilde{R}(t)$ (for convenience we temporarily drop the mode lables $(\mathbf{k}, \alpha)$):

$$\dot{a} + i\omega a = \tilde{R}(t) \tag{11}$$

From this point of view the test wave is driven by the ambient waves which act as an 'equilibrium heat bath.' It is convenient to transform variables, defining

$$b(t) = e^{i\omega t} a(t) \tag{12}$$

so that (11) becomes

$$\dot{b} = e^{i\omega t}\tilde{R} \equiv R(t) \tag{13}$$

Following the conventional argument [*Lax*, 1960, 1966], we suppose that at $t = 0$, b has the definite value $b(0)$. The mean of b, averaged over the ambient ensemble, obeys the equation

$$\frac{d}{dt}\langle b \rangle = \langle R(t) \rangle$$

It is anticipated that as $t \to \infty$, $\langle b \rangle \to 0$. This leads to a reasonable postulate for the form of R:

$$R(t) = -\nu b(t) + F(t), \qquad \langle F \rangle = 0 \tag{14}$$

Here ν is the Langevin relaxation rate (assumed real, since any imaginary part may be removed by a transformation of the form (12)).

From assumption (14), (13) becomes

$$\dot{b} + \nu b = F(t) \tag{15}$$

from which it follows that

$$\langle b(t) \rangle = b(0)e^{-\nu t} \tag{16}$$

To develop the fluctuation dissipation theorem we, assume that

$$\lim_{t\to\infty} \langle |b(t)|^2 \rangle = \sigma \tag{17}$$

a constant, 'equilibrium' value. (Since the hamiltonian from which (5) was derived has no lower bound in energy, a true equilibrium in the thermodynamic sense does not exist. However, large amplitude fluctuations are sufficiently rare that we can ignore this problem. Note the analogy with the theory of low-lying Stark states of hydrogen.) It is, of course, of interest to determine if the Garrett-Munk PSD (10) corresponds to this equilibrium, and this is one of the tasks for the computations in section 5.

Considerable simplification results by assuming δ correlation of the noise

$$\langle F(t)F^*(t') \rangle \cong 2D\delta(t - t') \tag{18}$$

where D is a real constant depending on the ambient spectrum. Numerical investigations described later indicate that the decorrelation time t_c is sufficiently small that (18) is a good approximation for our application.

Integration of (15) using assumptions (17) and (18) and restoring mode labels yields the fluctuation-dissipation result

$$\nu_F(\mathbf{k}, \alpha) = \frac{D(\mathbf{k}, \alpha)}{\sigma_{\mathbf{k}\alpha}} \tag{19a}$$

where the subscript F indicates that this relaxation rate constant is derived by the fluctuation-dissipation method.

For future comparison with the radiative transfer equation we generalize (19*a*) to define a (possibly time dependent) rate coefficient

$$\hat{\nu}_F(\mathbf{k}, \alpha) = \frac{D(\mathbf{k}, \alpha)}{\langle |a_{\mathbf{k}\alpha}|^2 \rangle} \tag{19b}$$

where $\langle |a_{\mathbf{k}\alpha}|^2 \rangle$ does not necessarily represent an equilibrium value.

To evaluate D we use the linear approximation for the ambient field amplitudes on the right-hand side of (5):

$$a_{l\beta}(t) = a_{l\beta}(0)e^{-i\omega_\beta t}$$

We also use the cumulant discard approximation to reduce fourth moments to second moments. Evaluation is straightforward, giving

$$D(\mathbf{k}, \alpha) = \frac{1}{2}\int_{-\infty}^{\infty} \langle F(t)F^*(0) \rangle \, dt$$

$$= \pi \sum_{l,m} \{ |G_m^{kl}|^2 \delta_{\mathbf{k}+\mathbf{l}-\mathbf{m}} \delta(\omega_\alpha + \omega_\beta - \omega_\gamma)$$

$$+ 2|G_{lm}^{k}|^2 \delta_{\mathbf{k}-\mathbf{l}-\mathbf{m}} \delta(\omega_\alpha - \omega_\beta - \omega_\gamma) \} \langle |a_{l\beta}|^2 \rangle \langle |a_{m\gamma}|^2 \rangle \tag{20}$$

For a large ocean area $\sum_0$ we may replace wave number sums by integrals with the substitution

$$\sum_{\mathbf{l}} \to \frac{\sum_0}{4\pi^2} \int d^2l$$

and use (20) and (9) to rewrite (19*b*):

$$\hat{\nu}_F(\mathbf{k}, \alpha) = 2\pi \sum_{\beta,\gamma} \int d^2l d^2m \{|G_m{}^{kl}|^2 \delta(\mathbf{k} + \mathbf{l} - \mathbf{m})\delta(\omega_\alpha + \omega_\beta - \omega_\gamma) + 2|G_{lm}{}^{k}|^2 \delta(\mathbf{k} - \mathbf{l} - \mathbf{m})\delta(\omega_\alpha - \omega_\beta - \omega_\gamma)\} \frac{l^2 m^2}{k^2} \times \frac{\psi(\mathbf{l}, \beta)\psi(\mathbf{m}, \gamma)}{\psi(\mathbf{k}, \alpha)} \quad (21)$$

It is clear that $\hat{\nu}_F$ is a positive quantity.

Perturbation Method

The Krylov-Bogoliubov-Mitropolsky two-time perturbation method [*Bogoliubov and Mitropolsky*, 1961] provides an alternative means of obtaining a Langevin equation of the form (15) (see, e.g., *Case* [1966]). For the lowest-order perturbation calculation the cumulant discard assumption is not required, since the test wave is a sure quantity at $t = 0$ under the averages. A straightforward calculation yields a complex test wave frequency

$$\Omega_\alpha(\mathbf{k}) = \omega_\alpha + \delta\omega(\mathbf{k}, \alpha) \quad (22)$$

The relaxation rate is then

$$\nu_F(\mathbf{k}, \alpha) = -\mathrm{Im}\,(\delta\omega(\mathbf{k}, \alpha))$$

$$= -2\pi \sum_{\beta,\gamma} \int d^2 l\, d^2 m \{2G_m{}^{kl} G_{lk}{}^{m} \delta(\mathbf{k} + \mathbf{l} - \mathbf{m})\delta(\omega_\alpha + \omega_\beta - \omega_\gamma) + G_l{}^{km} G_l{}^{mk*} \delta(\mathbf{k} - \mathbf{l} + \mathbf{m})\delta(\omega_\alpha - \omega_\beta + \omega_\gamma) + 2G_{lm}{}^{k} G_k{}^{ml} \delta(\mathbf{k} - \mathbf{l} - \mathbf{m})\delta(\omega_\alpha - \omega_\beta - \omega_\gamma)\} l^2 \psi(\mathbf{l}, \beta) \quad (23)$$

Radiative Transfer Equation

The radiative transfer or Boltzmann equation has been used by *Olbers* [1976] and *McComas and Bretherton* [1977] to describe nonlinear internal wave interactions. In this method the equations of motion (5) are used to obtain an equation for $d\langle|a_k|^2\rangle/dt$ (see, for example, *Davidson* [1972]) in terms of $\langle a_k a_l a_m{}^*\rangle$, etc. Equations for the rate of change of these third-order moments involve fourth moments. Closure results from discard of fourth-order cumulants, leaving second-order moments. Use of the homogeneity assumption allows expression of these in terms of the PSD. Finally, first-order perturbation theory is used to integrate the equations for $\langle a_k a_l a_m{}^*\rangle$. The result of all this is the transport equation

$$\frac{d}{dt}\langle|a_{k\alpha}|^2\rangle = 2\nu_B(\mathbf{k}, \alpha)\langle|a_{k\alpha}|^2\rangle \quad (24a)$$

where

$$\nu_B = \hat{\nu}_F - \nu_P \quad (24b)$$

The expressions (21) and (23) for $\hat{\nu}_F$ and ν_P are to be used here. Symmetry properties of the G coefficients may be used to rewrite (24) in precisely the form given by *Olbers* [1976] and *McComas and Bretherton* [1977] (Appendix B).

Equation (24) shows the relationship of the Boltzmann transport equation to the two versions of the Langevin description. We shall see in the next section that (24) may also be derived directly from the Langevin equations.

In the application of the fluctuation-dissipation theorem we were required to assume that the $\langle|a_{k\alpha}|^2\rangle$ corresponded to the equilibrium state $\sigma_{k\alpha}$. This was not, of course, used to obtain (23) and (24), which result from dynamical equations. We see from (24), however, that if $\langle|a_{k\alpha}|^2\rangle = \sigma_{k\alpha}$, then $\nu_B(\mathbf{k}, \alpha) = 0$ and

$$\hat{\nu}_F(\mathbf{k}, \alpha) = \nu_F(\mathbf{k}, \alpha) = \nu_P(\mathbf{k}, \alpha) \quad (25)$$

The two forms of the Langevin equation and the transport equation (24) are then consistent. In fact, if the spectrum is not a true equilibrium but merely a steady state ($\nu_B = 0$) for some region of $\mathbf{k} - \alpha$ space, (25) is still valid for that region. We have seen that the quantity $\hat{\nu}_F$ is always positive. Evidently, for a steady state, ν_P must also be positive, although this is not guaranteed, since the full expression (23) for ν_P is not positive definite.

When the ambient field is in (or near) a steady state, so $\nu_P > 0$, the fluctuation-dissipation "noise" D tends to excite the mode $(\mathbf{k}, \alpha)$ at a rate ν_F (or $\hat{\nu}_F$). Energy is lost to the ambient field at the rate ν_P. To illustrate the implications of this, suppose that our test wave has arbitrary initial amplitude, but all other modes are in a steady state. We can then use (19*b*) to integrate (24):

$$\langle|a_{k\alpha}(t)|^2\rangle = \langle|a_{k\alpha}(0)|^2\rangle e^{-2\nu_F t} + \frac{D}{\nu_P}(1 - e^{-2\nu_F t}) \quad (26)$$

The asymptotic value is evidently

$$\langle|a_{k\alpha}|^2\rangle = \frac{D(\mathbf{k}, \alpha)}{\nu_P(\mathbf{k}, \alpha)}$$

as required by the fluctuation-dissipation theorem and (25). Now, from (16), we obtain (for t large compared to t_c, the correlation time of the left hand side of (18))

$$\langle a_{k\alpha}(t) a_{k\alpha}{}^*(0)\rangle = \langle|a_{k\alpha}(0)|^2\rangle e^{-\nu_F t - i\omega_\alpha t} \quad (27)$$

So from (26), the time scale for $\langle|a_{k\alpha}|^2\rangle$ to reach equilibrium is determined by ν_P, while the autocorrelation function (27) decay rate is determined by ν_F.

The dynamical calculations reported in paper 1, corresponding to numerical integration of (5) seem to be reasonably consistent with (26). A test wave of initially small amplitude was found to grow to the GM-76 value in roughly the expected time. It remained at this level as long as the calculation was continued.

In the above discussion we have assumed the existence of a steady state solution to (24). For this to have physical interest the solution should correspond, to some extent, to observed internal wave spectra. In section 5 we shall present computed values of $\hat{\nu}_F$ and ν_P for a class of GM spectra and conclude as did *McComas and Bretherton* [1977] that GM-76 is nearly a steady state spectrum except for frequencies close to the inertial frequency and for the lowest mode numbers. Within the "steady state region" we will see that ν_B may be several orders of magnitude smaller than $\hat{\nu}_F$ and therefore tends to be quite sensitive to details of the spectrum.

4. Fokker-Planck Equation

The assumption that the noise term in (15) represents a Markoff process, fluctuating rapidly on the time scale t_c that is small compared to $\nu_F{}^{-1}$, permits one to derive a Fokker-Planck equation for the probability distribution of the amplitude b [*Chandrasekhar*, 1943; *Wang and Uhlenbeck*, 1945]. To obtain this, we first write b in terms of its real and imaginary parts, $b = x + iy$. The probability density for x and y at time t

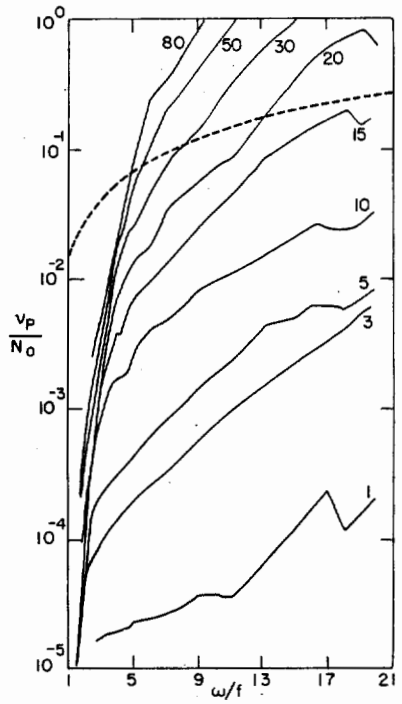

Fig. 1. Decay rate versus test wave frequency. Curves are labeled by mode number. Dashed curve represents $\nu_P = \omega_\alpha$. GM-76 is used.

is written as $P(x, y, t)$. The Fokker-Planck equation is obtained from (15):

$$\frac{\partial P}{\partial t} = \frac{\partial}{\partial x}[\nu_F x P] + \frac{\partial}{\partial y}[\nu_F y P] + \left(\frac{\partial^2}{\partial x^2} + \frac{\partial^2}{\partial y^2}\right)\left[\frac{DP}{2}\right] \tag{28}$$

Here D is the quantity defined by (20). An equation of evolution for the wave amplitude intensity

$$\langle |a|^2 \rangle = \int (x^2 + y^2) P \, dx \, dy$$

may be obtained immediately from (28):

$$\frac{d}{dt}\langle |a_{k\alpha}|^2 \rangle = 2\nu_F(\mathbf{k}, \alpha)[\sigma_{k\alpha} - \langle |a_{k\alpha}|^2 \rangle] \tag{29}$$

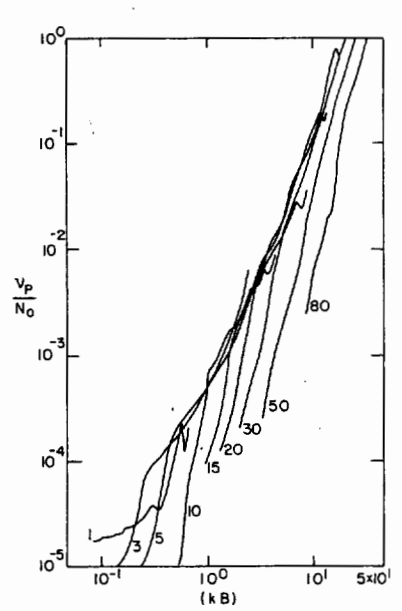

Fig. 2. Decay rate versus wave number for GM-76.

This is precisely equivalent to (24) if there exists an equilibrium spectrum σ, since then $\nu_F = \nu_P$.

We have now introduced three different rate constants, ν_P, ν_F, and ν_B. It is to be observed from (24), (26), (27), and (29) that ν_B describes the net rate of transfer of action (or energy), whereas ν_P (or ν_F) represents a relaxation rate.

5. Computations and Results

In this section we evaluate (21) and (23) for $\hat{\nu}_F$ and ν_P for given test wave parameters (wave number, frequency, and mode number). The coefficients G depend on integrals over WKB modefunctions $W_{k\alpha}$. In Appendix A we show that to a good approximation the mode number dependence of these integrals can be replaced by a delta function condition (corresponding to approximate vertical wave number conservation). This greatly simplifies the evaluation of the decay rates, since use of the delta functions reduce their calculation to a single sum over mode number (selects individual frequency resonance curves) and a single integral along each curve.

The parameter range for the calculations is determined by the region of validity of the WKB model. We allow frequencies in the range $f < \omega < N_0/3$, where the upper limit may be varied to test for sensitivity of results. If any member of a wave triad has a frequency greater than the cutoff value, that triad does not contribute to ν. Similarly, we employ a long wavelength cutoff at 100 km so that the 'plane ocean' assumption remains valid. For satisfactory convergence (~5%) of the values for ν it was sufficient to retain only mode numbers in a band of half width 25 centered about the test wave mode number. That is, triads lying on resonance curves for which $|\alpha - \beta|$, $|\alpha - \gamma| \leq 25$ were included in the calculations.

Changing the value of the frequency cutoff by 25% typically produce less than a 5% change in ν for frequencies $\omega_\alpha < 15f$. For higher frequencies, important local frequency and wave number interactions (induced diffusion, section 6) are blocked by the cutoff, and the rates are diminished. Quantitative results are found up to $\simeq 17f$ or even higher for large mode numbers. Changing the low–wave number cutoff can also have a significant effect (~factor of 2), especially for low mode numbers. This is again due to the induced diffusion mechanism where one triad member has a small wave number. The analysis in section 6 provides a semiquantitative estimate for the importance of this cutoff.

Figure 1 presents a plot of the decay rate ν_P against test

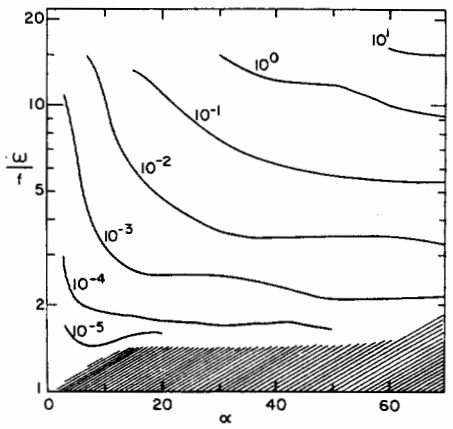

Fig. 3. Contours of ν_P/N_0 for GM-76. The shaded region indicates negative ν_P corresponding to test wave growth.

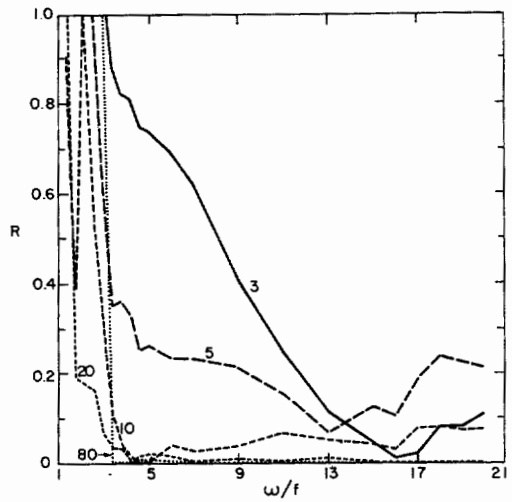

Fig. 4. Comparison of ν_B with $\hat{\nu}_F$. The quantity R (equation (30)) is plotted against test wave frequency for selected mode number. GM-76.

wave frequency for the GM-76 PSD (10). Each solid curve is labeled by the test wave mode number α. The heavy dashed curve represents equality between decay rate and linear frequency and therefore distinguishes regions of weak and strong nonlinearity (below and above the curve, respectively). Since the theory assumes a weakly nonlinear wavefield, little quantitative reliability can be placed on results above the dashed curve. The high-frequency 'kink' in the curves is a result of the frequency cutoff at $21f$.

The results show some common trends and features. For given test wave frequency, waves with large mode number (wave number) decay most rapidly: for given mode number, the higher-frequency (wave number) waves decay fastest, and there is a low-frequency threshold ($\omega_\alpha \simeq 3f$) below which the decay rate decreases very rapidly with decreasing frequency. These features are also exhibited in Figure 2, which presents the same results as Figure 1 except ν_P is plotted as a function of wave number. At high frequencies, a common (mode number independent) k dependence for the decay rate is apparent.

It was noted in section 3 that the expression (23) for ν_P is not positive definite: Interactions for which $\omega_\alpha = \pm(\omega_\beta - \omega_\gamma)$ ('difference reactions') have the possibility of giving rise to initial growth of the test wave amplitude. It is clear that if $\omega_\alpha < 2f$, difference reactions are the only type of interactions possible; therefore ν_P is most likely to be negative at these low frequencies. Indeed our results show growth (negative ν_P) for small frequencies, especially at high mode numbers. This is indicated in Figure 3, which is a contour plot of the rate calculations. Here the shaded region corresponds to growth, the remainder to decay.

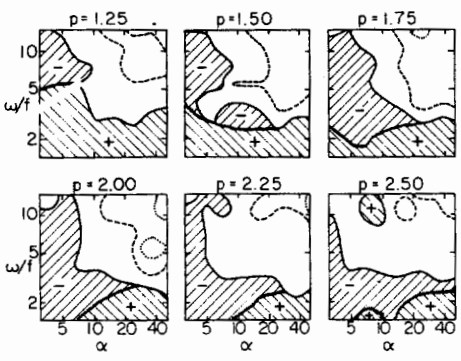

Fig. 5. Comparative steady states for different wave number slopes p of PSD (10). GM-76 uses $p = 2$. Nonsteady regions ($R > 0.1$) are shaded, and the sign of ν_B is given. Otherwise contours of R are drawn. Dashed contours denote $R = 10^{-2}$, dots denote $R = 10^{-3}$.

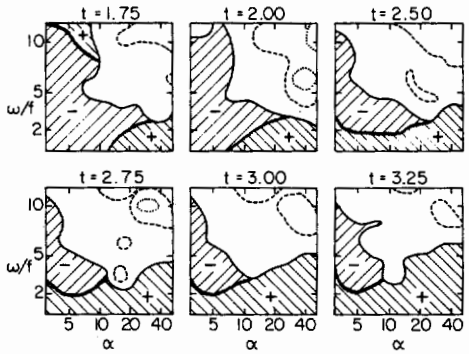

Fig. 6. Comparative steady states for different mode number slopes t of PSD (10). GM-76 uses $t = 2$.

The calculation of the fluctuation-dissipation decay rate $\hat{\nu}_F$ is essentially the same as for ν_P, and the same cutoff parameters were used. Numerical estimates of the correlation time t_c for the noise term F in (15) show that $t_c \sim \omega_\alpha^{-1}$, so that the delta correlation assumption (18) is valid in the same region as the weak nonlinearity assumption, $\hat{\nu}_F < \omega_\alpha$.

In section 3 we saw that if ψ is a steady state PSD for the mode $(\mathbf{k}, \alpha)$, then $\hat{\nu}_F(\mathbf{k}, \alpha) = \nu_P(\mathbf{k}, \alpha)$. Similarly, if the wave field is nearly a steady state, then $\nu_B = \hat{\nu}_F - \nu_P$ is 'small.' An appropriate measure of this is not ν_B itself but rather the ratio

$$R(\mathbf{k}, \alpha) \equiv \frac{|\nu_B|}{\hat{\nu}_F} \tag{30}$$

which compares the time scale for evolution of the spectrum to that for relaxation of a single mode.

The ratio R is plotted against ω_α for selected α in Figure 4 using the GM-76 PSD. Apart from a sharp increase in R at low frequencies and at high mode numbers (associated with $\nu_P < 0$), the small size of R over such a wide range of ω_α and α is supportive evidence that GM-76 is a 'good' representation of a steady state. Below we will compare GM-76 with other spectral forms to test the sensitivity of this result.

Olbers [1976] and *McComas and Bretherton* [1977] have calculated energy transfer rates for various GM models. They have also determined the direction of the energy flow by mapping regions of positive and negative ν_B. We investigate the effect of the variation of two parameters in the PSD. Using GM-76 as the basic form for ψ (see equation (10)), we change the wave number slope p and the mode number slope t.

Wave Number Slope Change

With the mode number slope given by the reference GM-76 value ($t = 2$) we compute the ratio R for six values of the wave number slope. The results are presented as contours in (ω_α, α) space in Figure 5. Regions for which $R > 0.1$ are designated 'nonsteady' and shaded to indicate the sign of ν_B. Energy flows from regions of negative (decay) to positive (growth) ν_B. When $R < 0.1$, contours of R are plotted, and the sign of ν_B is ignored. The area of this region and of the region $R < 0.01$ indicates how much of the spectrum is a steady state.

The GM-76 PSD ($p = 2$) is a steady state except for low mode numbers ($\alpha < 7$) where the action decays and for low frequencies and high mode numbers ($\omega < 2.5f$, $\alpha > 7$) where

the action grows. Decreasing p extends the $\nu_B > 0$ region to lower mode numbers and higher frequencies; increasing p has the opposite effect. Overall, GM-76 is closest to steady state in the high wave number region, although the results for smaller slopes are not very different.

Mode Number Slope Change

Here the procedure is the same as above except that the wave number slope is fixed at the GM-76 value ($p = 2$), and the mode number parameter t is varied. Figure 6 shows the results in the same format as Figure 5. Unlike the previous case, as t decreases, the growth region is confined to higher mode numbers, while the decay region expands. The GM-76 spectrum is again more closely a steady state for high wave numbers than the other spectra, although for $2 < t < 3$, there is little change in the steady state region.

Generally, the steady region $\alpha > 5$ and $\omega_\alpha > 3f$ is insensitive to the slope parameters p and t. However, these parameters strongly affect the division between regions of growth and decay of the action. For GM-76 our computations are in agreement with McComas and Bretherton, indicating that action flows from $\alpha \lesssim 5$ into $\alpha \gtrsim 10$ and $\omega_\alpha \lesssim 3f$.

6. Special Transfer Mechanisms

McComas and Bretherton [1977] have emphasized that certain classes of triads have significant roles in determining transfer rates. In this section we shall discuss quantitatively the importance of these mechanisms for both the Langevin and Boltzmann rate constants.

We begin with a discussion of the mechanisms called induced diffusion and elastic scattering by McComas and Bretherton. We discuss these together as limiting case 1 (LC1). As previously, we let $(\mathbf{k}, \alpha)$ be the test wave; then LC1 corresponds to the triad conditions

$$\omega_\gamma(m) \simeq \omega_\alpha(k) \gg \omega_\beta(l) \qquad m \simeq k \gg l \tag{31}$$

In this limiting case the G coefficients have simple forms, and we may rewrite (21), (23), and (24b) as

$$\nu_x(\mathbf{k}, \alpha) = \frac{\pi}{2} BN_0 \frac{[\omega_\alpha^2(k) - f^2]^2}{k^2} \sum_{\beta,\gamma} \frac{\omega_\gamma^2(k) - f^2}{\omega_\gamma(k)} \frac{A_x}{\psi(\mathbf{k}, \alpha)} \times \int_{l<k} d^2l\, \psi(\mathbf{l}, \beta) \frac{\omega_\beta^2(l)}{l^2} \nu_{\mathbf{k}\alpha,\mathbf{l}\beta,\mathbf{k}\gamma}^2 \sum_{\pm} \delta[\omega_\alpha(k) - \omega_\gamma(k) \pm \omega_\beta(l)] \tag{32}$$

The index x is used to represent P, F, or B, where

$$A_P \equiv \frac{N_0\omega_\alpha(k)}{\omega_\alpha^2(k) - f^2}\psi(\mathbf{k}, \alpha)$$

$$A_F \equiv \frac{N_0\omega_\gamma(k)}{\omega_\gamma^2(k) - f^2}\psi(\mathbf{k}, \gamma) \tag{33}$$

$$A_B \equiv A_F - A_P$$

From (6) and (9) it is seen that A_x is proportional to wave action. The quantity ν_{klk} is the overlap integral of vertical mode functions evaluated in Appendix A.

Equations (32) and (33) show that for LC1 triads the steady state condition $\nu_B = 0$ corresponds to

$$A_F = A_P \tag{34}$$

or that A be independent of mode number (equipartition of action). (For the case of induced diffusion this was noted by *McComas and Bretherton* [1977].) The results (32) and (34) do not require either the WKB or the Boussinesq approximations. The WKB dispersion relation (7) yields for (34)

$$\psi(\mathbf{k}, \alpha) \sim \alpha^{-1}$$

except near the inertial frequency, which is precisely the form of GM-76 (10) in this domain and for $\alpha \gg 3$. The numerical calculations in the previous section show a steady state in this same region. We shall see in the following that this is because LC1 triads dominate the wave interactions.

The integral ν_{klk} appearing in (32) is evaluated in the WKB approximation in Appendix A. From this we see that

$$\nu_{klk}^2 \propto [\delta_{\alpha-\beta-\gamma} + \delta_{\alpha+\beta-\gamma} + \delta_{\alpha-\beta+\gamma}] \tag{35}$$

(For our actual calculations we use the more accurate form given in the Appendix.) The terms $\beta = \pm(\alpha - \gamma)$ when $\gamma \simeq \alpha \gg \beta$ correspond to induced diffusion (ID). The term $\beta = \alpha + \gamma$ corresponds to elastic scattering (ES).

Analytic evaluation of (32) for these two cases gives the expressions

Induced diffusion

$$\frac{\nu_P}{N_0} = 6.4 \times 10^{-4} \frac{(\alpha - \frac{1}{4})^3(\beta - \frac{1}{4})^2\omega_\alpha}{(1 - (\pi\omega_\alpha/2N_0))^6\beta^2(\beta^2 + 9)N_0}$$

$$\beta = \frac{1}{4} + \frac{(\alpha - \frac{1}{4})f\omega_\alpha}{(\omega_\alpha^2 - f^2)}, \tag{36}$$

Elastic scattering

$$\frac{\nu_P}{N_0} = 1.0 \times 10^{-5} \frac{(kB)^3N_0^2\omega_\alpha}{(1 - (\pi\omega_\alpha/2N_0))^3} \times \sum_{+,-} \frac{(\beta - \frac{1}{4})^2}{\beta^2(\beta^2 + 9)(\omega_\gamma^2 - f^2)^{3/2}(1 - (\pi\omega_\gamma/2N_0))^3} \tag{37}$$

$$\beta = \tfrac{1}{4} + (\alpha - \tfrac{1}{4})\left\{1 + [(\omega_\alpha^2 - f^2)/(\omega_\gamma^2 - f^2)]^{1/2}\right\}$$

The sum '+,−' above represents the sum over the two cases

$$\omega_\gamma = \omega_\alpha(k) \pm f \tag{38}$$

For the analytic evaluation of (36) and (37) the upper limit of the integral over l in (32) has been taken to be infinity, since this has little effect on the result. The numerical calculations reported in section 5 use a lower limit $l_{\min} = 2\pi/(100\text{ km})$. If we incorporate this cutoff in our analysis, expressions (36) and (37) are multiplied by a factor

$$[1 - (2/\pi)\tan^{-1}(l_{\min}BN_0/\beta\pi f)]$$

In Figure 7 we compare the ID expression (36) (dashed curve) with the calculated numerical results (solid curve) for ν_P (for this comparison the l integral cutoff was included). It is evident that except for $f < \omega \lesssim 3f$, the ID mechanism provides a very good approximation for ν_P and that ν_P may be easily calculated from the analytic expression (36).

In Figure 8 we compare the ES (36) and ID (39) expressions for ν_P. It is seen that ES is much less important than ID. The ES mechanism was significant, however, for the 'up-down' asymmetry calculation of ν_B by *McComas* [1978], because his perturbed state was in approximate equilibrium for ID.

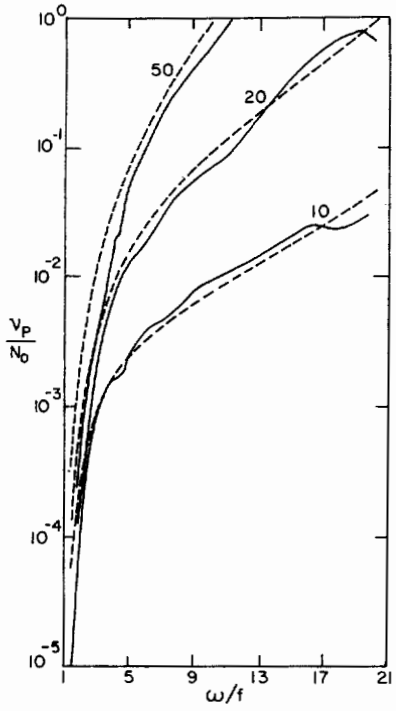

Fig. 7. Comparison between the dominant induced diffusion transfer mechanism (equation (36)) and the full numerical calculation of ν_P/N_0. Curves are labeled by mode number.

The parametric subharmonic instability (PSI) mechanism of *McComas and Bretherton* [1977] corresponds to a large-scale double-frequency wave interacting with two smaller-scale waves with nearly equal frequencies. In our notation, this corresponds to $\beta \ll \alpha, \gamma$,

$$\omega_\beta/2 \simeq \omega_\alpha \simeq \omega_\gamma \tag{39}$$

with no strong condition on wave number. Since the ID mechanism successfully accounts for the interactions with $\omega_\alpha \gtrsim 3f$, we expect that, at most, PSI could be important in the region $\omega_\alpha \lesssim 2f$. For this case we find

$$\nu_P \simeq -\nu_F \tag{40}$$

and an analytic evaluation is again possible. In contrast to the ID and ES derivations a finite upper limit must be imposed on the l wave number integration for convergence of the approximate expressions.

Choosing $l_{max} = k$, a rather crude approximation for ν_P in the range $f \le \omega_\alpha \le 2f$ can be derived which gives the correct order of magnitude:

$$\frac{\nu_P}{N_0} \simeq -\frac{\hat{\nu}_F}{N_0} \simeq -3.5\,(10)^{-7}\left(4-\frac{f^2}{\omega_\alpha^2}\right)^{5/2}[Q-\tan^{-1}Q]$$

$$Q = \frac{kBN_0}{\pi(4\omega_\alpha^2 - f^2)^{1/2}} \tag{41}$$

Values calculated from (41) are shown in Figure 8.

The main conclusions of this section are that for $\omega_\alpha > 3f$ and $\alpha \ge 5$ the ID mechanism expressed by (36) provides a good description of relaxation within the internal wave field. Equation (32), its analytic solution, and the good agreement with the full numerical calculation explain why the GM-76 spectrum is nearly a steady state in this domain. For a detailed discussion of the significance of the individual mechanisms we refer to *McComas and Bretherton* [1977].

7. Energy Flow

Three-wave interactions are only one of the many processes which contribute to the overall energy balance in the ocean. To understand the measured internal wave energy spectrum requires a quantitative measure of flow rates between the various sources and sinks. Here we obtain an estimate of the energy flow rate through the nonequilibrium region of GM-76 which also indicates the energy requirements to maintain the spectrum.

The mean energy per unit area $E(\mathbf{k}, \alpha)$ for the test wave is (paper 1, equation (2.19))

$$E(\mathbf{k}, \alpha) = \omega_\alpha(k)\langle J_{\mathbf{k}\alpha}\rangle \tag{42}$$

The flow rate is obtained by taking the time derivative of (42) using (24), (6), and (9):

$$\frac{dE(k,\alpha)}{dt} = \frac{4\pi^2}{\Sigma_0}\frac{2\omega_\alpha^2}{\omega_\alpha^2 - f^2}\nu_B\psi(\mathbf{k}, \alpha)\rho_0 N_0^2 B \tag{43}$$

Since the radiative transfer equation conserves total energy, the net energy flow from the region $\nu_B < 0$ is equal to the flow into $\nu_B > 0$. We compute the flow from the negative region by integrating (43) over this domain of k, α space:

$$\frac{dE^{(-)}}{dt} \equiv \sum_\alpha \frac{dE_\alpha^{(-)}}{dt} = \sum_\alpha \sum_{\mathbf{k}} \frac{dE(\mathbf{k}, \alpha)}{dt} \qquad \nu_B < 0 \tag{44}$$

The calculated partial rates $dE_\alpha^{(-)}/dt$ are given in Table 1 for mode numbers between $\alpha = 1$ and $\alpha = 6$. For the first 5 mode numbers they are comparable, while for $\alpha = 6$ the rate has decreased by nearly a factor of 2, and the contributions from $\alpha > 6$ (not shown) are much smaller. Except for $\alpha = 1$, the main contribution to the k sum in (44) peaks near $\omega_\alpha \simeq 2.2f$, independent of α. Although the peak is not sharp, it does suggest that the flow through the spectrum to smaller frequencies is weak. The major flow is from low to high mode numbers. The net energy flow rate from the region of negative ν_B

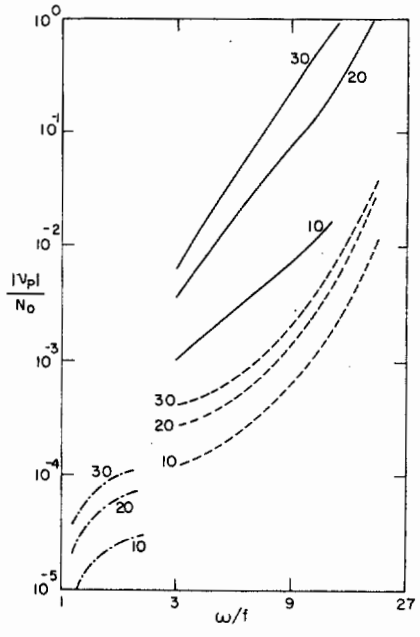

Fig. 8. Comparison of contributions to $|\nu_P|/N_0$ from special transfer mechanisms. Analytic expressions for induced diffusion (equation (36), solid curve), elastic scattering (equation (37), dashed curve), and parametric subharmonic instability (equation (41), dot-dash curve), are evaluated. Curves are labeled by mode numbers.

TABLE 1. Energy Flow Rates (W m^{-2}) From Low Mode Numbers

α	$-\frac{dE_\alpha^{(-)}}{dt} \times 10^4$
1	1.1
2	1.3
3	1.3
4	1.1
5	1.0
6	0.6

$$\frac{dE^{(-)}}{dt} = \sum_\alpha \frac{dE_\alpha^{(-)}}{dt} = -6.4\,(10)^{-4}\ \mathrm{W\,m^{-2}}$$

sums to $dE^{(-)}/dt \simeq 6.4\,(10)^{-4}$ W/m^2 for $\alpha \leq 6$, and we believe that this represents only a slight underestimate of the total rate.

Olbers [1976] has evaluated the transfer rate to high mode numbers for the GM-75 spectrum and found it to be $3\,(10)^{-3}$ Wm^{-2}, significantly larger than our GM-76 rate. *McComas and Bretherton* [1977], however, have noted a sensitivity of results to spectral shape, as is reflected in our Figures 5 and 6. Thus the validity of computed transfer rates certainly depends on the precision to which the spectrum is known.

Appendix A: Overlap Integrals for Exponential Profile

The explicit form of the coupling coefficients G in the equations of motion (5) is given in the appendix of paper 1. The only Väisälä profile dependent terms in these coefficients are the 'overlap integrals:'

$$\nu_{klm} = \frac{1}{\rho_0}\int_{-H}^{0} \rho W_{k\alpha}' W_{l\beta}' W_{m\gamma}'\, dz$$
$$\mu_{lm}{}^{k} = \frac{1}{\rho_0}\int_{-H}^{0} \rho W_{k\alpha}' W_{l\beta} W_{m\gamma}\, dz \tag{A1}$$

where the mode functions $W(z)$ are solutions of (4) with the normalization

$$\frac{1}{\rho_0}\int_{-H}^{0} (N^2 - f^2)\rho W_{k\alpha} W_{k\beta}\, dz = \delta_{\alpha,\beta} \tag{A2}$$

The Boussinesq approximation entails setting $\rho = \rho_0 = \rho(z = 0)$ in these integrals as well as in (4). Since typically ρ varies by only ~0.3% over the depth of the ocean, this approximation has little effect on the values of the overlap integrals (A1).

In this approximation the eigenvalue problem (4) becomes

$$W_{k\alpha}'' + Q_{k\alpha}{}^2(z) W_{k\alpha} = 0$$
$$Q_{k\alpha}{}^2 \equiv k^2\left(\frac{N^2(z) - \omega_\alpha{}^2}{\omega_\alpha{}^2 - f^2}\right) \tag{A3}$$

where $Q_{k\alpha}$ is the 'vertical wave number' as a function of depth.

If we restrict ourselves to the region $\omega \ll N_0$, the $\mu_{lm}{}^k$ integral can be neglected. Qualitatively this can be seen by considering the constant profile model

$$N = N_0 \qquad B < z < 0 \tag{A4}$$

for which

$$\nu_{klm} = \frac{1}{N_0{}^3(2B)^{1/2}} Q_\alpha Q_\beta Q_\gamma \{\delta_{\alpha-\beta-\gamma} + \delta_{\beta-\gamma-\alpha} + \delta_{\gamma-\alpha-\beta}\}$$
$$\mu_{lm}{}^{k} = \frac{1}{N_0{}^3(2B)^{1/2}} Q_\alpha \{-\delta_{\alpha-\beta-\gamma} + \delta_{\beta-\gamma-\alpha} + \delta_{\gamma-\alpha-\beta}\} \tag{A5}$$
$$Q_\alpha = \frac{\alpha\pi}{B}$$

From the form of the coupling coefficients (paper 1, equation (A.2)), it is seen that the ratio of the μ to the ν containing terms is given by

$$(k/Q)^2 \sim (\omega/N_0)^2 \ll 1$$

This result is confirmed quantitatively by numerical evaluation of the overlap integrals for the exponential profile.

To compute ν_{klm}, it is sufficient to use the WKB solutions of (A3) correct to first order in $\eta = \omega/N_0$:

$$W_{k\alpha}(z) = \left(\frac{2}{B}\right)^{1/2} \frac{1}{N_0}\frac{d_{k\alpha}}{Q_{k\alpha}(0)} e^{-z/2B} \sin\left[\phi(z) + \pi/4\right]$$

where

$$Q_{k\alpha}(z) = \frac{1}{B}\left[\frac{\Delta_\alpha}{1 - (\pi/2)\,\eta_\alpha}\right]\frac{N}{N_0} \qquad \Delta_\alpha \equiv \pi(\alpha - \tfrac{1}{4})$$
$$d_{k\alpha} \equiv \left[\frac{BQ_{k\alpha}{}^3(0)}{\Delta_\alpha + \frac{1}{2}}\right]^{1/2} \tag{A6}$$
$$\phi(z) = \left(\frac{N}{N_0} - 1\right)Q_{k\alpha}(0)B + \Delta_\alpha$$

The WKB overlap integral is formed by differentiating W_k, neglecting the derivative of the $e^{-z/2B}$ term, and substituting into (A1). The result is

$$\nu_{klm} = \frac{(-1)^{\alpha+\beta+\gamma}}{N_0{}^3(2B)^{1/2}} d_{k\alpha} d_{l\beta} d_{m\gamma} \{I_{lm}{}^{k} + I_{mk}{}^{l} + I_{kl}{}^{m}\} \tag{A7}$$

where

$$I_{lm}{}^{k} \equiv \left(\frac{\pi}{2q^3}\right)^{1/2} [C_2(q)\sin q - S_2(q)\cos q] \tag{A8}$$

Here S_2 and C_2 are Fresnel Integrals [*Abramowitz and Stegun*, 1964], and q is the dimensionless vertical wave number mismatch at the surface

$$q = B|Q_{k\alpha}(0) - Q_{l\beta}(0) - Q_{m\gamma}(0)| \tag{A9}$$

To first order in η this can be written as

$$q = \pi|\alpha - \beta - \gamma + \tfrac{1}{4} + \tfrac{1}{2}(\eta_\alpha\Delta_\alpha - \eta_\beta\Delta_\beta - \eta_\gamma\Delta_\gamma)| \tag{A10}$$

The function $I_{lm}{}^k$ is peaked about zero vertical wave number mismatch. This gives an approximate vertical wave number conservation law analogous to that in (A5) for the constant N model. Comparing (A7) with (A5) further shows that $d_{k\alpha}$ plays the role of effective vertical wave number.

A simple functional fit to $I_{lm}{}^k$ is given by

$$I_{lm}{}^{k}(q) = \tfrac{1}{3}e^{-aq^2}\cos(bq) \tag{A11}$$

where $a = 0.0453$ and $b = 0.3743$. It involves an error of less than 4% for $0 \leq q < 4$.

To facilitate the evaluation of the Langevin decay rates we approximate the function $I_{lm}{}^k$ with a delta function, thereby enabling one of the mode number summations in (22) and

(25) to be replaced by a trivial integral. Using expression (A11), it can be readily verified that the replacement

$$I_{lm}{}^{k} \approx \frac{1}{(2)^{1/2}}\,\delta(q) \tag{A12}$$

is valid.

Numerical computation of the overlap integrals using the exact Bessel function solutions [*Garrett and Munk*, 1972] show that the accuracy of (A7) decreases with increasing frequencies reaching 40% at $\omega/N_0 \sim 0.25$ (providing the mode numbers are greater than 1). For $q = 0$ the $\mu_{lm}{}^{k}$ are typically less than 20% of the $B^2\nu_{klm}$; however, as q increases, ν decreases rapidly (see (A11)), while μ is relatively constant.

The relation of the eigenmode formulation used here to the vertically propagating wave description of *Olbers* [1976] and of *McComas and Bretherton* [1977] is seen with the construction of wave packets. We choose a position z_0 and an interval $|z - z_0| \le L_\nu/2$. The $a_{k\alpha}$'s may be replaced with a new set of coefficients b_{kP}, defined within the interval L_ν, with the relation

$$i \sum_{\alpha} N_0(B)^{1/2} W_{k\alpha}(z) a_{k\alpha} = -\sum_{n} e^{iPz} b_{kP} \Delta(z - z_0) \tag{A13}$$

Here

$$\Delta(z - z_0) = 1 \qquad |z - z_0| < \frac{L_\nu}{2}$$

$$\Delta(z - z_0) = 0 \qquad |z - z_0| > \frac{L_\nu}{2}$$

and

$$P \equiv P(n) = \frac{2\pi n}{L_\nu} \qquad n = 0, \pm 1, \pm 2, \cdots$$

Equation (A13) may be 'solved' for either the $a_{k\alpha}$ or the b_{kP} using (A2) or the relation

$$\int dz\, \Delta(z - z_0) e^{i(P - P')z} = L_\nu \delta_{P,P'}$$

With the approximation (A12) it is straightforward to reexpress (5) with the $(\mathbf{k}, P)$ labels.

Appendix B: Alternative Expressions for Relaxation Rates

Equations (21) and (23) can be rewritten in a form which makes transparent their relationship both to one another and to the familiar radiative transport equation of *Olbers* [1976], *McComas and Bretherton* [1977], and *Davidson* [1972].

To do this we use the hamiltonian coupling coefficients $\Gamma_1(k; l, m)$ defined in paper 1 (Appendix) and also the wave action variables (6). In terms of these the relaxation rates are

$$\langle J_{k\alpha}\rangle \hat{\nu}_P(\mathbf{k}, \alpha) = 4\pi \sum_{\beta,\gamma} \sum_{l,m} \{\tfrac{1}{2}|\Gamma_1(k; l, m)|^2 \delta_{k-l-m}\delta(\omega_\alpha - \omega_\beta - \omega_\gamma) + |\Gamma_1(m; k, l)|^2 \delta_{k+l-m}\delta(\omega_\alpha + \omega_\beta - \omega_\gamma)\} \langle J_{l\beta}\rangle \langle J_{m\gamma}\rangle \tag{B1}$$

$$\langle J_{k\alpha}\rangle \nu_P(\mathbf{k}, \alpha) = 4\pi \sum_{\beta,\gamma} \sum_{l,m} \{\tfrac{1}{2}|\Gamma_1(k; l, m)|^2 \delta_{k-l-m}\delta(\omega_\alpha - \omega_\beta - \omega_\gamma) \times (\langle J_{l\beta}\rangle + \langle J_{m\gamma}\rangle)\langle J_{k\alpha}\rangle + |\Gamma_1(m; l, k)|^2 \delta_{k+l-m}\delta(\omega_\alpha + \omega_\beta - \omega_\gamma) \times (\langle J_{l\beta}\rangle - \langle J_{m\gamma}\rangle)\langle J_{k\alpha}\rangle\} \tag{B2}$$

Substitution of these expressions into ν_B (24*b*) yields the usual expression.

Acknowledgments. This research was partially supported by the Office of Naval Research under contract N00014-78-C-0050. The authors wish to express appreciation to W. H. Munk and P. Yau for helpful discussions.

References

Abramowitz, M., and I. A. Stegun, *Handbook of Mathematical Functions*, National Bureau of Standards, Gaithersburg, Md., 1964.

Bogoliubov, N. N., and Y. A. Mitropolsky, *Asymptotic Methods in the Theory of Nonlinear Oscillations*, Gordon and Breach, New York, 1961.

Cairns, J. L., and G. O. Williams, Internal waves from a midwater float, 2, *J. Geophys. Res., 81*, 1943–1950, 1976.

Case, K. M., A general perturbation method for quantum mechanical problems, *Prog. Theor. Phys. Suppl., 37/38*, 1966.

Chandrasekhar, S., Stochastic problems in physics and astronomy, *Rev. Mod. Phys., 15*, 1–89, 1943.

Davidson, R. C., *Methods in Nonlinear Plasma Theory*, pp. 133–173, Academic, New York, 1972.

Garrett, C. J. R., and W. H. Munk, Space-time scales of internal waves, *Geophys. Fluid Dyn., 2*, 225–264, 1972.

Garrett, C. J. R., and W. H. Munk, Space-time scales of internal waves: A progress report, *J. Geophys. Res., 80*, 291–297, 1975.

Garrett, C. J. R., and W. H. Munk, Internal waves in the ocean, in *Annual Review of Fluid Mechanics*, edited by M. Van Dyke, J. V. Wehousen, and J. L. Lumley, Annual Reviews, Inc., Palo Alto, Calif., 1979.

Hasselmann, K., Feynman diagrams and interaction rules of wave-wave scattering processes, *Rev. Geophys. Space Phys., 4*, 1–32, 1966.

Hasselmann, K., Nonlinear interactions treated by the methods of theoretical physics, *Proc. Roy. Soc. London, Ser. A, 299*, 77–100, 1967.

Holloway, G., and M. Hendershott, Stochastic closure for nonlinear Rossby waves, *J. Fluid Mech., 82*, 747–765, 1977.

Lax, M., Fluctuations from the nonequilibrium steady state, *Rev. Mod. Phys., 32*, 25–64, 1960.

Lax, M., Classical noise, IV, Langevin methods, *Rev. Mod. Phys., 38*, 541–566, 1966.

McComas, C. H., Equilibrium mechanisms within the oceanic internal wave field, *J. Phys. Oceanogr., 7*, 836–845, 1978.

McComas, C. H., and F. P. Bretherton, Resonant interaction of oceanic internal waves, *J. Geophys. Res., 82*, 1397–1412, 1977.

Meiss, J. D., N. Pomphrey, and K. M. Watson, Numerical analysis of weakly nonlinear wave turbulence, *Proc. Nat. Acad. Sci. U.S., 76*, 2109–2113, 1979.

Olbers, D. J., Non-linear energy transfer and the energy balance of the internal wave field in the deep ocean, *J. Fluid Mech., 74*, 375–399, 1976.

Phillips, O. M., *The Dynamics of the Upper Ocean*, Cambridge University Press, New York, 1977.

Wang, M. C., and G. E. Uhlenbeck, On the theory of the Brownian motion, *Rev. Mod. Phys., 17*, 323–342, 1945.

(Received May 14, 1979;
revised September 12, 1979;
accepted September 28, 1979.)